Excess Loss in Homodyne Detection Originating from Distributed Photocarrier Generation in Photodiodes

Takahiro Serikawa and Akira Furusawa[*]

Department of Applied Physics, School of Engineering, The University of Tokyo, 7-3-1 Hongo, Bunkyo-ku, Tokyo 113-8656, Japan

The distributed absorption of photons in photodiodes induces an excess noise in continuous-wave photodetection above the transit-time roll-off frequency. We show that it can be treated as a frequency-dependent excess optical loss in homodyne detection. This places a limit on the bandwidth of high-accuracy homodyne detection, even if an ideal photodetector circuit is available. We experimentally evaluate the excess loss in two ways: a comparison of signal gain and shot-noise gain of one-port homodyne detection and a balanced homodyne detection of squeezed light at a 500-MHz sideband. These results agree with an analytic expression we develop, where the randomness of the photoabsorption is directly modeled by an intrusion of vacuum field. At 500 MHz, we estimate the excess loss at 14% for a Si photodiode with 860-nm incident light, while the numerical simulation predicts much smaller excess loss in (In, Ga)As photodiodes with 1550 nm light.

I. INTRODUCTION

Optical homodyne detection [1–3] is a key technology in photonic quantum communication and computation such as continuous-variable (CV) quantum key distribution [4] or CV measurement-based computation [5–7], since it offers high-speed, high-precision quantum measurement. For these applications, optical loss in the interferometer or the photodiode must be kept low to avoid mixing the target quantum observable with vacuum noise. Even a few percents of loss can be a fatal issue in the struggle to exceed the quantum error correction threshold [8]. Also, any other noises in the detection process degrade the signal and can cause errors in the quantum protocols. For the future practical applications of homodyne detection, it is especially challenging but important to realize high-speed detectors while avoiding losses and noises. Recent development of highly efficient, high-speed, low-noise homodyne detectors has realized wideband detectors with more than a 100-MHz bandwidth [9,10] or a narrowband detector whose center frequency is as high as 500 MHz [11]. In principle, the bandwidth of homodyne detectors is not limited by the cutoff of the photodiodes or detector circuits because it can be canceled by postprocessing equalizers. The signal-to-noise ratio is the true limiting factor, while it can be possibly improved by cryogenic amplifiers that have quite a low noise level. Here a question arises: what is the

fundamental limit of the bandwidth of quantum homodyne detection?

Sun *et al.* pointed out [12] that distributed absorption or randomness in photocarrier transport in photodiodes causes excess photocurrent noise. This excess noise becomes an intrinsic limit of the signal-to-noise ratio of photodetection in the high-frequency domain. They showed that carrier scattering is the major factor of the excess noise for (In, Ga)As uni-traveling-carrier photodiodes over 10 GHz and it increases the timing jitter of the detection of ultrashort optical pulses.

This mechanism also takes place in continuous-wave (CW) photodetection, leading to a broadband noise limit in homodyne detection. In this paper, we introduce a simple model using a series beam-splitter picture and show that the randomness of the distributed absorption is described by a frequency-dependent optical loss. We experimentally examine the loss spectrum of Si-PIN (positive intrinsic negative) photodiodes in two ways: shot-noise spectrum measurement and squeezed light measurement. We show that the distributed absorption is dominant in the excess noise of Si-PIN photodiodes with a thick absorption layer and that the excess loss is not ignorable above the 100-MHz region. This is an urgent problem for the forthcoming broadband optical quantum-information processing and suggests a need for considerations in the applications on quantum key distribution or metrology. We expect that the excess loss depends on the material of photodiodes, which provides new design criteria for high-efficiency photodiodes.

_____
[*]akiraf@ap.t.u-tokyo.ac.jp

II. MODEL

A. Noise in Homodyne detection

Optical homodyne detection [1,2] can be considered as demodulation of a signal light field with a local oscillator (LO) at the carrier light frequency. In an ideal situation, the photocurrent signal I is proportional to the quadrature amplitude of the signal field and homodyne detection is a projection measurement of a quadrature operator $\hat{x}$. When the signal light is a vacuum, the random arrival of LO photons, i.e., shot noise, is interpreted as vacuum fluctuation of $\hat{x}$. I is normalized by the shot-noise amplitude $\sqrt{\langle I_{\text{shot}}^2 \rangle}$, which is usually done in the frequency domain as $x(\omega) = I(\omega)/\sqrt{\langle I_{\text{shot}}(\omega)^2 \rangle}$ for the compensation of the frequency-dependent gain of the detector. Here, a convenient way of treating extra Gaussian noise in the detection process such as the electric noise of the detector is to include it in the shot noise and the normalization procedure in homodyne detection reinterprets the extra noise as a vacuum noise, i.e., an optical loss [13]. The excess noise originating from the distributed photocarrier generation or random carrier transport is also to be regarded as an optical loss, since the excess noise has Gaussian distribution due to the central limit theorem for the average of numerous photons in the LO.

B. Effect of distributed absorption on homodyne detection

We consider a photodetection with a simple PIN photodiode. The input light photons are transformed to electron-hole pairs in the intrinsic region at random penetration depth, which has exponential decay distribution $f(x) = \alpha e^{-\alpha x}$, where α is the absorption coefficient. The carrier transport of each photocarrier pair generates photocurrent at the electrode, which has a position-dependent impulse response function $h(t; x)$ (Fig. 1). Here, $h(t; x)$ is assumed to be a deterministic function and the randomness in the transport such as recombination or scattering is ignored, so
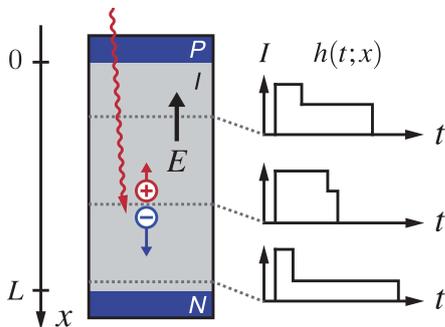
FIG. 1. Illustration of distributed photocarrier generation in a PIN photodiode. Position-dependent photocurrent impulse responses $h(t; x)$ are shown at different absorption positions.

the distributed absorption of photons is the only factor of excess noise.

The frequency-ω component of the homodyne detection corresponds to the quadrature observable of a sideband field $\hat{x}(\omega)$ [14]. In Appendix A, we derive the spectral characteristics of the photocurrent signal of homodyne detection under the existence of distributed absorption. As shown in Eq. (A7), the frequency-ω component of the lock-in detected photocurrent is given as a sum of $\hat{x}(\omega)$ and a noise term, reading

$$\hat{I}(\omega) \propto A(\omega)\hat{x}_{\text{in}}(\omega) + B(\omega)\hat{x}_{\text{vac}}(\omega), \qquad (1)$$

where

$$A(\omega) = \left| \int_0^L dx\, e^{-\alpha x} H(\omega; x) \right|, \qquad (2)$$

$$B(\omega) = \sqrt{\frac{1}{\alpha} \int_0^L dx\, e^{-\alpha x} \left| H(\omega; x) - \alpha e^{\alpha x} \int_x^L dx'\, e^{-\alpha x'} H(\omega; x') \right|^2}, \qquad (3)$$

and $H(\omega; x)$ is the Fourier transform of $h(t; x)$, $\hat{x}_{\text{vac}}(\omega)$ is a vacuum state quadrature operator, and L is the thickness of the photodiode. In Eq. (1), $[A(\omega)]^2$ is the signal gain spectrum, which shows roll-off due to the transit time of the carrier drift. $[B(\omega)]^2$ is the gain of the vacuum noise term, which expresses the excess noise originating from the distributed absorption of photons.

Since the power spectrum of shot noise is given by $[A(\omega)]^2 + [B(\omega)]^2$, the normalization with the shot-noise power gives the equivalent optical loss of homodyne detection as

$$\mathcal{L}(\omega) = \frac{[B(\omega)]^2}{[A(\omega)]^2 + [B(\omega)]^2}. \qquad (4)$$

If $H(\omega; x)$ is invariant with x, $\mathcal{L}(\omega)$ reduces to e^{-Lx}, expressing the rate of photons that penetrate the intrinsic region. In the limit of $L \to \infty$, such loss vanishes in $\mathcal{L}(\omega)$. Even in this limit, a nonuniform impulse response $H(\omega; x)$ can result in a residual of the vacuum term. Since the excess loss is caused by the variation of the transfer functions respective to the absorption positions, it is nonzero only above the frequency where the transit-time roll-off takes place [12]. Note that photodiodes with high quantum efficiency must have enough thickness, and the excess loss term inevitably appears because of the distributed absorption within the absorption distribution $e^{-\alpha x}$, which is characteristic of the photodiode material.

C. Simulation of excess loss

The photocurrent impulse response $h(t; x)$ is obtained by the carrier transport dynamics and the Shockley-Ramo theorem [15,16]. The following assumptions are

reasonable when we consider PIN photodiodes with a thin P- and N-doped layer, high reverse-bias voltage, low illumination, low frequency, and low I-layer doping condition. (1) Absorption and carrier transport in a P- and N-doped contact layer can be ignored. (2) Carrier transport is dominated by drift in the depletion region; diffusion, recombination, and scattering contribute little to the photocurrent. (3) Electric field E is constant over the I layer as $E = V/L$, where V is the reverse-bias voltage; donor concentration is small and the space-charge effect of photocarriers can be ignored. Then the photocurrent is driven by electrons and holes drifting at constant velocities, leading to a simple formation of $h(t;x)$:

$$h(t;x) = \frac{q}{L}\left[v_{p}(E)\Theta(t)\Theta\left(\frac{x}{v_{p}(E)} - t\right) \right.$$
$$\left. + v_{e}(E)\Theta(t)\Theta\left(\frac{L-x}{v_{e}(E)} - t\right) \right], \qquad (5)$$

where q is elementary charge, $\Theta(t)$ is the Heaviside step function, and $v_{e,p}(E)$ is the drift velocity of electrons or holes as functions of the electric field.

Based on Eq. (5), we calculate the excess loss of PIN photodiodes that have near-unity quantum efficiency. The excess loss spectrum $\mathcal{L}(\omega)$ of Si with 860-nm light and that of $In_{0.47}Ga_{0.53}As$ with 1550-nm light are shown in Fig. 2. Here, we assume vertical incidence of the input light and ignore the effects of auxiliary layers such as contact layers or buffer layers. In the calculation, the following electrical and optical properties of Si or $In_{0.47}Ga_{0.53}As$ are used: electronic field dependence of the carrier velocities of Si [17] and $In_{0.47}Ga_{0.53}As$ [18,19], absorption coefficient of Si at 300 K [20], and absorption coefficient of $In_{0.47}Ga_{0.53}As$ at 300 K [21].

All the traces in Fig. 2 approach zero at low frequency because the transfer functions $H(\omega;x)$ become independent from x. High bias voltage increases the carrier velocity and thereby reduces the excess loss. However, there is a limit due to the saturation of carrier velocity and thus the minimum loss spectrum is governed by the absorption coefficient and the saturated carrier velocity of the semiconductor material. Si-PIN photodiodes can be considered as lossless below 100 MHz and (In, Ga)As-PIN photodiodes work well up to 1 GHz, because of its larger absorption coefficient.
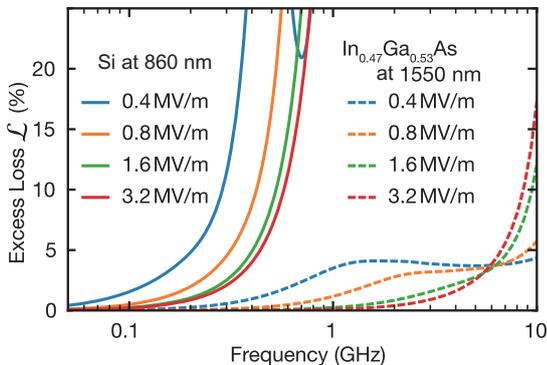
III. EXPERIMENT

We experimentally verify the above model in the following two ways. We use 860-nm CW light and a Si-PIN photodiode S5971SPL (Hamamatsu Photonics), which has near-unity quantum efficiency at 860 nm and whose active diameter is 0.8 mm. In both cases, 100-V reverse-bias voltage is applied to S5971SPL. The saturation characteristics of these photodiodes is separately measured and we confirm that 1-mW input power induces little saturation below 1 GHz. The experimental setup is shown in Fig. 3 and the details are described in Appendix B.
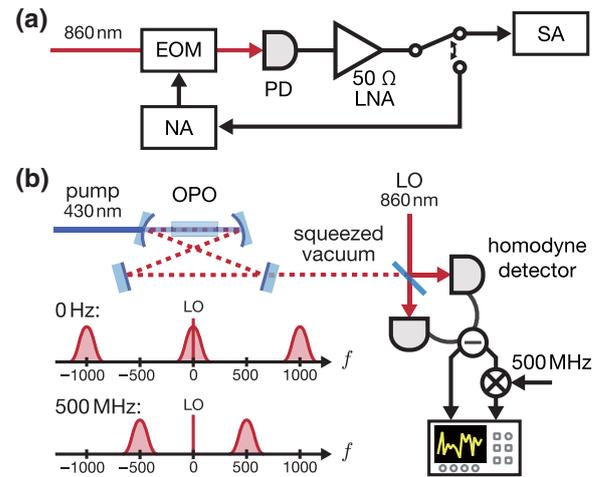
FIG. 3. Schematic of the experimental setups. (a) Shot noise and modulation measurement, with electro-optic modulator (EOM), network analyzer (NA), spectrum analyzer (SA), and low-noise amplifier (LNA). Here, 1 mW of CW light at 860 nm is detected by a S5971SPL photodiode. In the measurement of shot noise, the network analyzer is disconnected and the power spectrum is obtained by the spectrum analyzer. Modulation signal gain is measured by the amplitude modulator and the network analyzer. (b) Squeezed light measurement, with optical parametric oscillator (OPO) and local oscillator (LO). The OPO is pumped by a 430-nm CW pump and generates a squeezed vacuum at either 0 Hz or 500 MHz. The quadrature of the squeezed-vacuum state is measured by homodyne detection with a carrier frequency LO and the output signal is digitized by an oscilloscope. The resonance structure of the OPO is also shown for the measurement at 0 Hz and 500 MHz.

FIG. 2. Simulated excess loss spectrum $\mathcal{L}(\omega)$ at different electric fields E of a 100-μm-thick Si-PIN photodiode and a 10-μm-thick (In, Ga)As-PIN photodiode.

A. Comparison of shot-noise gain with modulation-signal gain of a photodiode

Here, we consider a one-port homodyne measurement of the vacuum state, which is essentially a single-eye detection of a laser beam. In Eq. (1), the power spectrum of the input signal $|\hat{x}_{in}|^2$ is expressed as $[A(\omega)]^2$ and the shot-noise spectrum is given by $[A(\omega)]^2 + [B(\omega)]^2$. By comparing these spectra, the ratio of $A(\omega)$ and $B(\omega)$ indicates the loss spectrum $\mathcal{L}$ as Eq. (4). These spectra are directly observed by a power spectrum measurement of a single photodiode with continuous light [Fig. 3(a)]. Here, a very fast photodiode S5973 (Hamamatsu Photonics) with 50-V reverse bias is used as a reference to calibrate the nonflat gain of the amplifiers, transmission lines, spectrum analyzer, network analyzer, and electro-optic modulator. The S5971SPL's spectrum is divided by the corresponding spectrum of S5973. Figure 4 shows the normalized gain spectrum and theoretical curves. The difference between the shot-noise spectrum and signal gain spectrum shows the existence of the excess loss. It is difficult to obtain a precise value of loss, since it is technically challenging to keep a high signal-to-noise ratio of the shot noise over 1 GHz, and the slight error in power calibration can be considerable in the amount of loss. The simulation curves of $[A(\omega)]^2 + [B(\omega)]^2$ and $[A(\omega)]^2$ well agree with the experimental data below 600 MHz. The negative gain peak at 800 MHz corresponds to a negative peak of the photocurrent transfer functions $H(\omega; x)$. The mismatch at higher frequency is due to the simplification in Eq. (5), where each hole and electron current impulse is a rectangular function, corresponding to the transfer function as a sinc function. We suppose the assumption that E is constant over the space-charge region of the photodiode is not accurate enough to describe the gain characteristics around the negative peak frequency.

B. Measurement of squeezed light at a high-frequency sideband

A convenient way of measuring the optical loss of photodiodes is to do a homodyne measurement of squeezed light [22], because the squeezing level is very sensitive to the absolute value of the detection efficiency. Here, we conduct a balanced homodyne measurement of a squeezed vacuum at 500 MHz, which is generated by an optical parametric oscillator (OPO). The OPO has the free spectral range of 1.0012 GHz and is locked so that it is resonant at ±500.6 MHz. A parametric process caused by a CW pump light at 430 nm produces squeezed light at a 500.6-MHz double sideband around the 860-nm carrier frequency, where, in principle, a pure squeezed state is obtained [23]. The purity of the measured squeezed state shows the total amount of losses in the setup. For a high signal-to-noise ratio in the homodyne measurement of the quadrature at 500.6 MHz, a resonant-type homodyne detector that equips
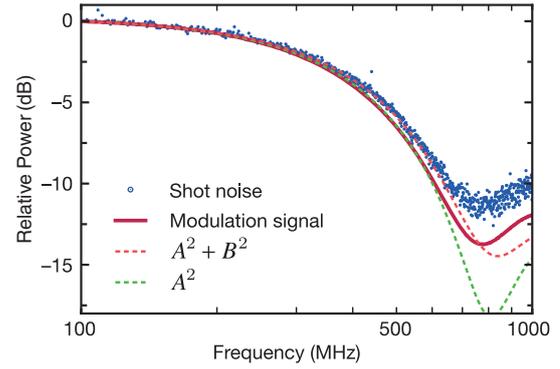
FIG. 4. Normalized power spectrum of the shot-noise and modulation signal gain of S5971SPL with 1-mW input power. Theoretical curves are calculated by Eqs. (1) and (5), with the parameters $L = 100 \ \mu$m, $V = 100$ V.

two S5971SPLs [11] is used. The LO light is 2 mW of CW light at 860 nm; thus, each S5971SPL has 1 mW of input power. To calibrate loss other than the photodiode's high-frequency loss, the squeezing level at 0 Hz is also measured. Since most of the loss factors, such as the OPO's internal loss, propagation loss, interference loss at homodyne detection, and imperfect quantum efficiency of the photodiode, are common at 0 Hz and 500 MHz, we can precisely cancel them by comparing the squeezing levels of these measurements.

Figure 5 shows the phase scan plot of the quadrature variance of squeezed light at 500 MHz and 0 Hz. The quadrature variance $V(\theta; \omega)$ normalized by the shot-noise variance is expressed as

$$V(\theta; \omega) = \mathcal{L}(\omega) + [1 - \mathcal{L}(\omega)] \left[\cos^2 \theta R(\omega) + \frac{\sin^2 \theta}{R(\omega)} \right],$$

(6)
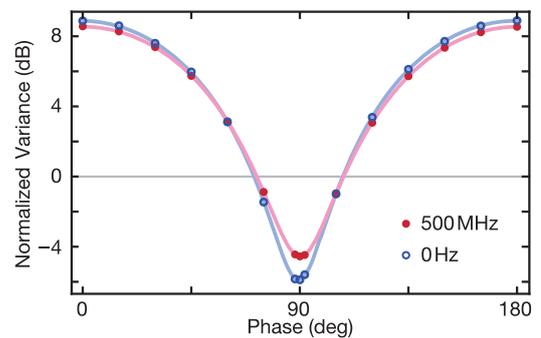
FIG. 5. Quadrature variance of the squeezed light at different frequencies. The narrow-band component around the center frequency within 300 kHz to 1 MHz is used for the calculation of variance. Statistical uncertainty is smaller than the diameter of points. Fitting curves are calculated using Eq. (6).

TABLE I. Summary of optical loss in the squeezed light measurement setup. The quantum efficiency of the photodiodes is an estimated value from the squeezed light measurement at 0 Hz. Note that the total optical loss $\mathcal{L}_{tot}$ is calculated from individual losses $\mathcal{L}_k$ as $\mathcal{L}_{tot} = 1 - \prod_k (1 - \mathcal{L}_k)$.

Loss factor	0 Hz	500 MHz
Propagation loss	3.5%	3.5%
Escape efficiency of OPO	2.7%	2.8%
Mode match at homodyne interferometer	6.8%	6.5%
Gain imbalance in homodyne detection	0.0%	0.0%
Probe light tapping	3.0%	1.7%
Photodiode quantum efficiency	1.7%	1.7%
Total	16.6%	15.3%

where θ is the phase of the quadrature operator and $R(\omega)$ is the initial squeezing level at ω. From the fitting in Fig. 5, the optical loss $\mathcal{L}(\omega)$ is estimated at 16.6% at 0 Hz and 27.4% at 500 MHz, and the initial squeezing level $R(\omega)$ is 9.06 dB at 0 Hz and 9.47 dB at 500 MHz. The individually measured losses of the setup are summarized in Table I.

Here, the quantum efficiency of the photodiode S5971SPL is estimated at 98.3% to make it consistent with the total loss of the squeezed light measurement at 0 Hz. The difference between the estimated total loss in the squeezed light measurement and the individually measured loss is 14.2% at 500 MHz, which is attributed to the excess optical loss of the photodiode. We assume about 0.5% of uncertainty in the estimation of the excess loss considering the fluctuation in the calibration.

C. Summary of the measurement and simulation of the excess loss of S5971SPL

The excess loss spectra of S5971SPL estimated by the two methods are shown in Fig. 6. The simulation based on Sec. C is also shown. The measured values of the excess loss roughly agree at 500 MHz. The broadband spectrum of the excess loss shows a characteristic peak around 800 MHz, where Eq. (5) become less reliable around such frequency as we observed in Fig. 4.

For Si photodiodes at 860 nm, our model well describes the excess loss and, thus, the distributed absorption is dominant in the excess noise. This is because Si has a low absorption coefficient, which gives rise to a large variation in the transfer function $H(\omega; x)$ with respect to x within the deep absorption region. Photodiode materials with a large absorption coefficient have a smaller effect of distributed absorption and other factors such as carrier scattering may give a contribution to the excess loss. In this sense, the model curves in Fig. 2 underestimate the excess loss, especially for the (In,Ga)As photodiode. A complete prediction of the excess loss can be given by the Monte Carlo simulation of photocarrier generation and transportation [12].
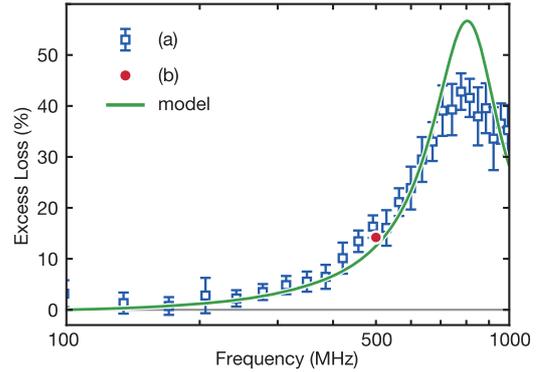
FIG. 6. Spectrum of the excess loss of S5971SPL. Blue square points: Excess loss calculated from the shot-noise measurement of S5971SPL. Red circle: Excess loss estimated from the squeezed light measurement. Green line: Theoretical curve from the model in Sec. C, with the same parameters as Fig. 4.

The 1-mW input power is small enough to avoid the effect of saturation of the photodiodes. For the high signal-to-noise ratio homodyne detection, a higher LO power is preferred; with a high illumination, however, the space-charge effect [24] may reduce the bias field and increase the excess loss. This can be easily avoided by broadening the aperture of the photodiodes, though.

In the experiment, the bias field in the photodiode is as large as 1 MV/m, and the carrier velocity is close to the saturation. There is thus not much room for reducing the excess loss by increasing the reverse bias (see Fig. 2). With a thinner absorption layer, the effect of the distributed absorption and carrier transit time can be suppressed. For example, cavity-enhanced photodiodes [25] can realize a high quantum efficiency with a very thin absorption layer. With the current technology, however, it is difficult to obtain near-100% quantum efficiency with such a photodiode structure. Therefore, our PIN photodiode model gives the practical upper limit of the frequency of high-efficiency photodetection.

IV. CONCLUSION

The distributed photon absorption in photodiodes causes excess noise in the high-frequency region of continuous-wave light detection. We formulate the excess noise by a beam-splitter model of random photodetection, where the noise is reinterpreted as an optical loss. The excess loss in a high-frequency region can be a critical limitation in the bandwidth of homodyne detection. We evaluate the impact of the excess loss for Si and (In,Ga)As photodiodes and show that it becomes non-negligible above 100 MHz and 1 GHz, respectively. We experimentally verify the excess loss of Si photodiodes by signal gain measurement and squeezed light measurement. These results show agreement with the theoretical model.

At the 860 nm band, the material of high-efficiency photodiodes is practically limited to Si and the excess loss is not ignorable above 100 MHz. For the faster quantum homodyne detection, we would have to choose another photodiode material and the corresponding wavelength to work on. Another way of increasing the bandwidth of quadrature measurement is to add a parametric amplifier before homodyne measurement to conceal the loss or the noise in the photodetection [26,27], but it is nonetheless technically challenging to suppress the loss in the parametric amplification.

APPENDIX A: FORMULATION OF EXCESS LOSS

1. Beam-splitter model of distributed photocarrier generation

By slicing the absorber with the small width ξ, the photocarrier generation distribution is modeled by a series of beam splitters with reflectance $r = 1 - e^{-\alpha\xi}$, followed by virtual photon detectors with unity quantum efficiency. Vacuum field $\hat{a}_k^{\text{vac}}$ gets into the virtual detectors from the back ports of the beam splitters through the transmissivity of $1 - r$, representing the randomness of absorption positions.

Randomness other than the distributed absorption, such as carrier scattering in the photocarrier transport, can increase the excess noise. (Note that recombination is usually included in the evaluation of quantum efficiency.) Our model does not include such noises, but they can also be modeled by a set of beam splitters and impulse responses, which is eventually summarized into the excess loss.

The annihilation operator of the incident field at the kth photon detector is written as

$$\hat{A}_k(t) = \sqrt{r}(1-r)^{(k-1)/2}\hat{a}_{\text{in}}(t)$$
$$- r \sum_{l=1}^{k-1}(1-r)^{(k-l-1)/2}\hat{a}_l^{\text{vac}}(t)$$
$$+ \sqrt{1-r}\,\hat{a}_k^{\text{vac}}(t), \tag{A1}$$

where $\hat{a}_{\text{in}}(t)$ is the annihilation operator of the input field. The propagation delay in the semiconductor layer is ignored here. The kth photon detector has the photon-to-current impulse response $h(t;k\xi)$ and the output signal is its convolution with the photon number operator $\hat{A}_k^\dagger(t)\hat{A}_k(t)$. The output photocurrent $\hat{I}(t)$ is the sum of each detector's signal, reading

$$\hat{I}(t) = \int d\tau \sum_{k=1}^{M} \hat{A}_k^\dagger(\tau)\hat{A}_k(\tau)h(t-\tau;k\xi). \tag{A2}$$

The upper bound M of the sum is determined so that $L = M\xi$ is equal to the total thickness L of the intrinsic layer of the photodiode.

2. Excess loss in homodyne detection

For optical quadrature measurement, we consider one-port homodyne measurement [28] by introducing the large displacement a_0 to the incident field as $\hat{a}_{\text{in}}(t) = a_0 + \hat{a}_{\text{sig}}(t)$, where $\hat{a}_{\text{sig}}(t)$ is a small signal field operator. Balanced homodyne measurement is straightforwardly derived from one-port homodyne measurement [1] when the local-oscillator power and the photocurrent response is well balanced, because the excess noise terms are independent for each photodiode.

Taking the first-order term of a_0 in Eq. (A2) and ignoring the dc offset, we have

$$\frac{\hat{I}(t)}{a_0} = \int d\tau \sum_{k=1}^{M} \sqrt{r(1-r)^k}[\hat{a}_k^\dagger(\tau) + \hat{a}_k(\tau)]$$
$$\times h(t-\tau;k\xi). \tag{A3}$$

A Fourier transform of Eq. (A3) yields

$$\frac{\hat{I}(\omega)}{a_0} = \sum_{k=1}^{M} \sqrt{r(1-r)^k}[\hat{a}_k^\dagger(\omega) + \hat{a}_k(\omega)]H(\omega;k\xi), \tag{A4}$$

where $\hat{a}(\omega) = \int dt\, e^{-i\omega t} a(t)$ is the frequency-mode annihilation operator and $H(\omega;x) = \int dt\, e^{-i\omega t} h(t;x)$ is the position-dependent transfer function. The ac component of the quadrature signal is given by the lock-in detection of $\hat{I}(t)$. Here, we focus on the in-phase component of the demodulated signal $\hat{I}_{\text{I}}(\omega) \equiv [\hat{I}(\omega) + \hat{I}(-\omega)]/2$. Then, the in-phase photocurrent expresses the quadrature amplitude of a double-sideband mode:

$$\frac{\hat{I}_{\text{I}}(\omega)}{a_0} = r \left| \sum_{k=1}^{M}(1-r)^{k-1}H(\omega;k\xi) \right| \hat{x}_{\text{in}}^{\theta_\omega}(\omega)$$
$$- \sqrt{r} \sum_{k=1}^{M} \left| (1-r)^{k/2}H(\omega;k\xi) \right. \tag{A5}$$
$$\left. - r \sum_{l=k}^{M}(1-r)^{1-k/2}H(\omega;l\xi) \right| \hat{x}_k(\omega),$$

$$\theta_\omega = \arg\left[\sum_{k=1}^{M}(1-r)^{k-1}H(\omega;k\xi) \right], \tag{A6}$$

where $\hat{x}_{\mathrm{in}}^{\theta}(\omega) \equiv [e^{-i\theta}\hat{a}_{\mathrm{in}}^{\dagger}(-\omega) + e^{i\theta}\hat{a}_{\mathrm{in}}(\omega)]/2$ is the quadrature operator of the sideband field [29] at ω and $\hat{x}_{k}^{\theta}(\omega) \equiv [e^{-i\theta}\hat{a}_{k}^{\dagger}(-\omega) + e^{i\theta}\hat{a}_{k}(\omega)]/2$ is the quadrature operator of the back-port vacuum field, which is invariant with θ. By taking the limit of $\xi \to 0$, the above equations become

$$\frac{\hat{I}_{\mathrm{I}}(\omega)}{a_0} = A(\omega)\hat{x}_{\mathrm{in}}^{\theta_{\omega}}(\omega) + B(\omega)\hat{x}_{\mathrm{vac}}(\omega), \qquad \text{(A7)}$$

$$\theta_{\omega} = \arg \int_0^L dx e^{-\alpha x} H(\omega; x), \qquad \text{(A8)}$$

where $A(\omega)$ and $B(\omega)$ are given by Eqs. (2) and (3), and the vacuum noise terms are represented by a single vacuum operator $\hat{x}_{\mathrm{vac}}(\omega)$ using the relationship

$$\lim_{\xi \to 0} \sqrt{\xi} \sum_{k} f(k\xi)\hat{x}_k(\omega) = \sqrt{\int dx|f(x)|^2} \hat{x}_{\mathrm{vac}}(\omega) \quad \text{(A9)}$$

for vacuum operators $\hat{x}_k(\omega)$ and a real function $f(x)$. By omitting the explicit notation of the sideband phase θ_{ω}, Eq. (A7) reduces to Eq. (1). The quadrature-phase component of the sideband signal $\hat{I}_{\mathrm{Q}}(\omega) \equiv [\hat{I}(\omega) - \hat{I}(-\omega)]/2i$ is similarly derived as

$$\frac{\hat{I}_{\mathrm{Q}}(\omega)}{a_0} = A(\omega)\hat{x}_{\mathrm{in}}^{\theta_{\omega}+\pi/2}(\omega) + B(\omega)\hat{x}_{\mathrm{vac}}'(\omega), \qquad \text{(A10)}$$

where $\hat{x}_{\mathrm{vac}}'(\omega)$ is another vacuum operator that is independent of $\hat{x}_{\mathrm{vac}}(\omega)$.

APPENDIX B: DETAILS OF THE EXPERIMENT

1. Comparison of shot-noise gain with intensity modulation signal gain of a photodiode

CW laser light at 860 nm is produced by a Ti:sapphire laser MBR-110 (Coherent). It is filtered by two mode-cleaning cavities to reduce the intensity noise above 10 MHz down to the shot-noise level. The photodetector is composed of a series of 50 Ω-input low-noise amplifiers HMC8410 (Analog Devices), which has the noise figure of 1.1 dB, and ZFL-1000LN+ (Minicircuits). The power spectrum of the shot-noise signal is obtained by a spectrum analyzer E4402B (Agilent Technologies) with a resolution bandwidth of 300 kHz and an average count of 1000. The raw trace data of the shot-noise spectra are shown in Fig. 8. We just replaced the photodiode from S5971SPL to S5973 on the detector board to take the two traces with the same electric gain. In Fig. 4, the circuit noise is subtracted from the shot-noise power. The signal-to-noise ratio of the shot-noise signal of S5971SPL is smaller than 5 dB above 500 MHz; this is why the uncertainty of the noise-subtracted
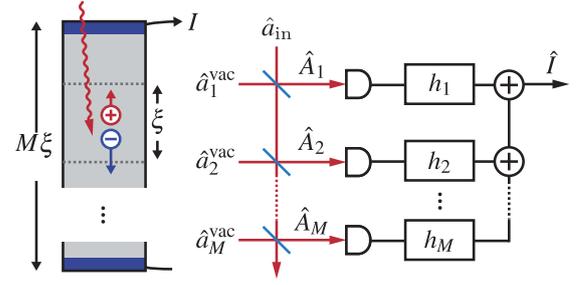
FIG. 7. Model of distributed photocarrier generation in the space-charge region of photodiodes. The incident field $\hat{a}_{\mathrm{in}}$ is probabilistically absorbed in virtually separated thin layers with the thickness ξ. The tapped field $\hat{A}_k$ at the kth beam splitter triggers photocurrent impulses $h_k(t) = h(t; k\xi)$.

shot-noise power gets large at a high frequency. The sharp peaks in the traces are the intensity noise of a 110-MHz modulation and its harmonics in the laser light. We eliminated these peaks from the data for the statistical processing for Fig. 6. The modulation signal gain is measured by a network analyzer E5080A (Keysight Technologies) and a waveguide intensity modulator (EOSPACE).

2. Measurement of squeezed light at high-frequency sideband

The OPO is a bow-tie-type cavity with a type-0 phase-matched periodically-poled KTiOPO$_4$ crystal (Raicol Crystals). The reflectivity of the output coupler is 88% and the linewidth of the OPO cavity is 10 MHz. The OPO is locked by a Pound-Drever-Hall method with a counterpropagating locking beam, which is detuned at a certain frequency to produce squeezed light at the specific frequencies. The oscillation threshold of the OPO is measured at 550 mW and the pump power is set at 100 mW, corresponding to the normalized pump amplitude 0.43. The relative phase between the pump and the LO is locked during the acquisition. The measurement setups of the 0-Hz squeezed light measurement and the 500-MHz
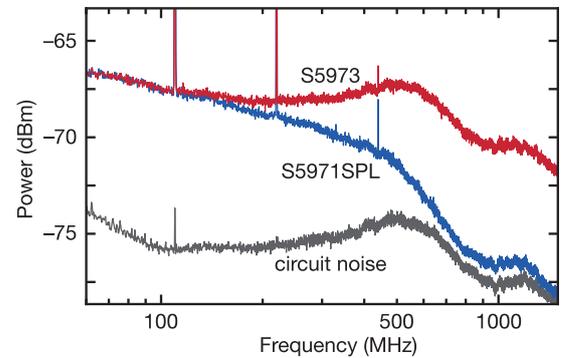
FIG. 8. Shot-noise spectrum detected by S5971SPL and S5973. The circuit noise of the detector is also shown.
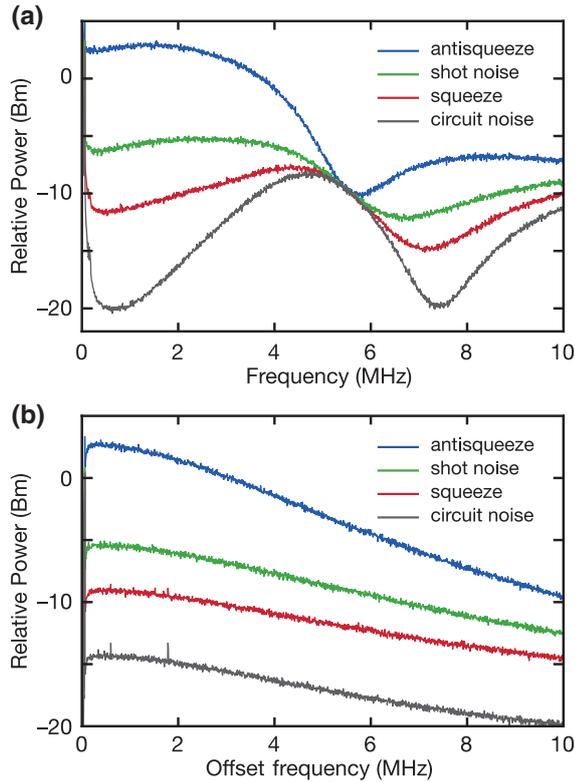
FIG. 9. Power spectrum of squeezed or antisqueezed light at (a) 0 Hz and (b) 500 MHz. The shot-noise level and circuit-noise level are also shown.

squeezed light measurement are slightly different and they are separately described below.

The output signal of the homodyne detection is digitized by a 12-bit oscilloscope DSOS204A (Keysight Technologies) with the sampling rate of 200 MHz and duration of 150 us. The power spectra are obtained by the fast Fourier transform and are averaged over 1000 frames of the traces for each LO phase. The power spectra of the squeezed light are shown in Fig. 9. In Fig. 5, the averages of the power spectrum from 300 kHz to 1 MHz are shown, where the circuit noise power is subtracted from the signals in the frequency domain.

3. Squeezed light measurement at 500 MHz

The OPO-locking beam is detuned at 1.5018 GHz. To probe the pump phase, a reference light with a modulation at ± 500.6 MHz generated by an EOM is introduced from the high-reflection port of the OPO. The reference modulation component is downconverted to 0 Hz by an EOM placed on the output beam. A triangle-shaped frequency separator cavity extracts the 0-Hz component, which is subsequently detected for the feedback control of the pump phase. The modulation causes 1.7% of optical loss in the

in-phase component of the squeezed light at 500.6 MHz, which is taken into account in Table I. The gain and phase balance of the homodyne detection is precisely adjusted and we obtain 40 dB of intensity signal cancellation in the LO. Here, the arm lengths of beams are well matched and the gains of the photodiodes at 500 MHz are slightly tuned by adjusting the reverse voltage: 102.5 or 97.5 V are applied at each S5971SPL. The signal-to-noise ratio of the shot noise against the circuit noise is roughly 9 dB over the measured frequency range. The output of the homodyne detector is processed by an IQ demodulator ADL5380 (Analog Devices) with a 500.6-MHz electric LO to obtain the in-phase component of the sideband signal. Note that the power transfer of the reference light down-conversion depends on the sideband phase: the quadrature phase component of the 500.6-MHz sideband signal undergoes one third of the loss of the in-phase component. We avoid the mixing of these phase components by choosing the in-phase component by matching the demodulation phase with the down-conversion phase.

4. Squeezed light measurement at 0 Hz

The OPO-locking light is detuned at 1.012 GHz. A reference light is introduced at 0 Hz from the high-reflection port of the OPO. The reference light is tapped by a partial-reflection mirror with 97% reflectivity in place of the frequency separator cavity, which causes 3.0% of the optical loss on the squeezed light. All the other optics are the same as those of the 500-MHz squeezed light measurement. The EOMs are electrically turned off. The dc output of the homodyne detector is directly digitized by the oscilloscope with the same configuration. The dc signal is affected by the resonant circuit in the homodyne detector and the gain spectrum has a unique shape, as shown in Fig. 9.

[1] Horace P. Yuen, and Vincent W. S. Chan, Noise in homodyne and heterodyne detection, Opt. Lett. **8,** 177 (1983).
[2] Bonny L. Schumaker, Noise in homodyne detection, Opt. Lett. **9,** 189 (1984).
[3] M. J. Collett, R. Loudon, and C. W. Gardiner, Quantum theory of optical homodyne and heterodyne detection, J. Mod. Opt. **34,** 881 (1987).
[4] Artur K. Ekert, Quantum Cryptography based on Bell's Theorem, Phys. Rev. Lett. **67,** 661 (1991).
[5] Daniel Gottesman, Alexei Kitaev, and John Preskill, Encoding a qubit in an oscillator, Phys. Rev. A **64,** 012310 (2001).
[6] Stephen D. Bartlett, and William J. Munro, Quantum Teleportation of Optical Quantum Gates, Phys. Rev. Lett. **90,** 117901 (2003).
[7] Nicolas C. Menicucci, Peter van Loock, Mile Gu, Christian Weedbrook, Timothy C. Ralph, and Michael A. Nielsen,

Universal Quantum Computation with Continuous-Variable Cluster States, Phys. Rev. Lett. **97,** 110501 (2006).

[8] Nicolas C. Menicucci, Fault-Tolerant Measurement-based Quantum Computing with Continuous-Variable Cluster States, Phys. Rev. Lett. **112,** 120504 (2014).

[9] R. Kumar, E. Barrios, A. MacRae, E. Cairns, E. H. Huntington, and A. I. Lvovsky, Versatile wideband balanced detector for quantum optical homodyne tomography, Opt. Commun. **285,** 5259 (2012).

[10] Huang Duan, Fang Jian, Wang Chao, Huang Peng, and Zeng Gui-Hua, A 300-MHz bandwidth balanced homodyne detector for continuous variable quantum key distribution, Chin. Phys. Lett. **30,** 114209 (2013).

[11] Takahiro Serikawa, and Akira Furusawa, 500 MHz resonant photodetector for high-quantum-efficiency, low-noise homodyne measurement, Rev. Sci. Instrum. **89,** 063120 (2018).

[12] Wenlu Sun, Franklyn Quinlan, Tara M. Fortier, Jean-Daniel Deschenes, Yang Fu, Scott A. Diddams, and Joe C. Campbell, Broadband Noise Limit in the Photodetection of Ultralow Jitter Optical Pulses, Phys. Rev. Lett. **113,** 203901 (2014).

[13] Jürgen Appel, Dallas Hoffman, Eden Figueroa, and A. I. Lvovsky, Electronic noise in optical homodyne tomography, Phys. Rev. A **75,** 035802 (2007).

[14] F. A. S. Barbosa, A. S. Coelho, K. N. Cassemiro, P. Nussenzveig, C. Fabre, M. Martinelli, and A. S. Villar, Beyond Spectral Homodyne Detection: Complete Quantum Measurement of Spectral Modes of Light, Phys. Rev. Lett. **111,** 200402 (2013).

[15] William Shockley, Currents to conductors induced by a moving point charge, J. Appl. Phys. **9,** 635 (1938).

[16] Simon Ramo, Currents induced by electron motion, Proc. IRE **27,** 584 (1939).

[17] Simon M. Sze, *Semiconductor Devices: Physics and Technology* (John Wiley & Sons, Hoboken, 2001).

[18] V. Balynas, A. Krotkus, A. Stalnionis, A. T. Gorelionok, N. M. Shmidt, and J. A. Tellefsen, Time-resolved, hot-electron conductivity measurement using an electro-optic sampling technique, Appl. Phys. A **51,** 357 (1990).

[19] Sadao Adachi, *Physical properties of III-V semiconductor compounds* (John Wiley & Sons, Hoboken, 1992).

[20] Martin A. Green, and Mark J. Keevers, Optical properties of intrinsic silicon at 300 K, Progr. Photovoltaics: Res. Appl. **3,** 189 (1995).

[21] Sadao Adachi, Optical dispersion relations for GaP, GaAs, GaSb, InP, InSb, $Al_xGa_{1-x}As$, and $In_{1-x}Ga_xAs_yP_{1-y}$, J. Appl. Phys. **66,** 6030 (1989).

[22] Henning Vahlbruch, Moritz Mehmet, Karsten Danzmann, and Roman Schnabel, Detection of 15 db Squeezed States of Light and their Application for the Absolute Calibration of Photoelectric Quantum Efficiency, Phys. Rev. Lett. **117,** 110801 (2016).

[23] A. E. Dunlop, E. H. Huntington, C. C. Harb, and T. C. Ralph, Generation of a frequency comb of squeezing in an optical parametric oscillator, Phys. Rev. A **73,** 013817 (2006).

[24] Keith J. Williams, Ronald D. Esman, and Mario Dagenais, Effects of high space-charge fields on the response of microwave photo detectors, IEEE Photonics Technol. Lett. **6,** 639 (1994).

[25] M. Selim Ünlü, and Samuel Strite, Resonant cavity enhanced photonic devices, J. Appl. Phys. **78,** 607 (1995).

[26] U. Leonhardt, and H. Paul, High-Accuracy Optical Homodyne Detection with Low-Efficiency Detectors: 'Preamplification' from Antisqueezing, Phys. Rev. Lett. **72,** 4086 (1994).

[27] Yaakov Shaked, Yoad Michael, Rafi Z. Vered, Leon Bello, Michael Rosenbluh, and Avi Pe'er, Lifting the bandwidth limit of optical homodynemeasurement with broadband parametric amplification, Nat. Commun. **9,** 609 (2018).

[28] Michael Vasilyev, Sang-Kyung Choi, Prem Kumar, and G. M. D'Ariano, Investigation of the photon statistics of parametric fluorescence in a traveling-wave parametric amplifier by means of self-homodyne tomography, Opt. Lett. **23,** 1393 (1998).

[29] Carlton M. Caves, and Bonny L. Schumaker, New formalism for two-photon quantum optics. I. quadrature phases and squeezed states, Phys. Rev. A **31,** 3068 (1985).